Geophysical Research Letters

RESEARCH LETTER
10.1029/2022GL101985

Low-Altitude UAV Imaging Accurately Quantifies Eelgrass Wasting Disease From Alaska to California

Bo Yang[1], Timothy L. Hawthorne[2], Lillian Aoki[3,4], Deanna S. Beatty[5], Tyler Copeland[2], Lia K. Domke[6], Ginny L. Eckert[6], Carla P. Gomes[7], Olivia J. Graham[3], C. Drew Harvell[3], Kevin A. Hovel[8], Margot Hessing-Lewis[9], Leah Harper[10], Ryan S. Mueller[11], Brendan Rappazzo[7], Luba Reshitnyk[9], John J. Stachowicz[5], Fiona Tomas[12], and J. Emmett Duffy[10]

[1]Department of Urban and Regional Planning, San Jose State University, San Jose, CA, USA, [2]Department of Sociology and College of Sciences GIS Cluster, University of Central Florida, Orlando, FL, USA, [3]Department of Ecology and Evolutionary Biology, Cornell University, Ithaca, NY, USA, [4]Data Science Initiative, University of Oregon, Eugene, OR, USA, [5]Department of Evolution and Ecology, University of California Davis, Davis, CA, USA, [6]College of Fisheries and Ocean Sciences, University of Alaska Fairbanks, Juneau, AK, USA, [7]Department of Computer Science, Cornell University, Ithaca, NY, USA, [8]Department of Biology, San Diego State University, San Diego, CA, USA, [9]Near-shore Marine Ecology, Hakai Institute, Heriot Bay, BC, Canada, [10]MarineGEO Program and Smithsonian Environmental Research Center, Edgewater, MD, USA, [11]Department of Microbiology, Oregon State University, Corvallis, OR, USA, [12]Instituto Mediterráneo de Estudios Avanzados, CSIC-UIB, Esporles, Spain

Key Points:

- First study using low-altitude high-resolution unoccupied aerial vehicle (UAV) imagery to detect coastal seagrass disease spanning 18 degrees of latitude
- The low altitude UAV mapping achieved 1.5 cm spatial resolution and the object-oriented analysis were performed at the seagrass leaf scale
- Statistical validation against in situ sampling demonstrated reliable results to use drone imaging for coastal plants disease assessments

Citation:

Yang, B., Hawthorne, T. L., Aoki, L., Beatty, D. S., Copeland, T., Domke, L. K., et al. (2023). Low-altitude UAV imaging accurately quantifies eelgrass wasting disease from Alaska to California. *Geophysical Research Letters*, *50*, e2022GL101985. https://doi.org/10.1029/2022GL101985

Received 2 NOV 2022
Accepted 24 JAN 2023

Author Contributions:

Conceptualization: Bo Yang, C. Drew Harvell, Luba Reshitnyk, John J. Stachowicz, J. Emmett Duffy
Data curation: Bo Yang, Tyler Copeland, Lia K. Domke, Ginny L. Eckert, Carla P. Gomes, Olivia J. Graham, Margot Hessing-Lewis, Leah Harper, Ryan S. Mueller, Brendan Rappazzo, Luba Reshitnyk, Fiona Tomas
Formal analysis: Bo Yang, Tyler Copeland, Lia K. Domke, Ginny L. Eckert, Olivia J. Graham, Kevin A. Hovel, Leah Harper, Luba Reshitnyk, John J. Stachowicz, Fiona Tomas
Funding acquisition: C. Drew Harvell, John J. Stachowicz, J. Emmett Duffy

Abstract Declines in eelgrass, an important and widespread coastal habitat, are associated with wasting disease in recent outbreaks on the Pacific coast of North America. This study presents a novel method for mapping and predicting wasting disease using unoccupied aerial vehicles (UAVs) with low-altitude autonomous imaging of visible bands. We conducted UAV mapping and sampling in intertidal eelgrass beds across multiple sites in Alaska, British Columbia, and California. We designed and implemented a UAV low-altitude mapping protocol to detect disease prevalence and validated against in situ results. Our analysis revealed that green leaf area index derived from UAV imagery was a strong and significant (inverse) predictor of spatial distribution and severity of wasting disease measured on the ground, especially for regions with extensive disease infection. This study highlights a novel, efficient, and portable method to investigate seagrass disease at landscape scales across geographic regions and conditions.

Plain Language Summary Diseases of marine organisms are increasing in many regions worldwide, therefore, efficient time-series monitoring is critical for understanding the dynamics of disease and examining its progression in time to implement management interventions. In the first study of its kind, we use high-resolution unoccupied aerial vehicle (UAV) imagery collected to detect disease at 12 sites across the North-East Pacific coast of North America spanning 18 degrees of latitude. The low altitude UAV visible-bands imagery achieved 1.5 cm spatial resolution, and analysis was performed at the seagrass leaf scale based on object-oriented image analysis. Our findings suggest that drone mapping of coastal plants may substantially increase the scale of disease risk assessments in nearshore habitats and further our understanding of seagrass meadow spatial-temporal dynamics. These can be scaled up by searching for environmental signals of the pathogen, for example, with surveillance of wastewater for signs of Covid in human populations. This application could easily apply to other areas to construct a high-resolution monitoring network for seagrass conservation.

1. Introduction

Pathogens play an important role in the ecology of natural and human-dominated ecosystems worldwide (Lopez-Calderon et al., 2016). Iconic species from plants and corals to amphibians and mammals are increasingly suffering declines due to pathogenic organisms (Harvell et al., 2002). Disease outbreaks are increasing in frequency due to climate change, changes in species distributions, and interactions among these factors (Burge et al., 2014). However, a major challenge in understanding the ecology and impact of disease in all populations from plants to humans is developing a robust system for quantifying the prevalence and severity of infections and their impact (Glidden et al., 2022). Outbreaks are often not recognized until they are well underway, hampering mitigation measures. Yet the intensity with which surveillance must occur to detect outbreaks and the scale of spread often exceed available resources (Burge et al., 2016). Thus, the ability to characterize the spatial extent

Investigation: Bo Yang, John J. Stachowicz, J. Emmett Duffy
Methodology: Bo Yang, Ginny L. Eckert, Carla P. Gomes, Olivia J. Graham, Margot Hessing-Lewis, Brendan Rappazzo, J. Emmett Duffy
Project Administration: Ginny L. Eckert, C. Drew Harvell, Kevin A. Hovel, John J. Stachowicz, J. Emmett Duffy
Resources: Bo Yang, Lia K. Domke, Carla P. Gomes, Olivia J. Graham, C. Drew Harvell, Kevin A. Hovel, Margot Hessing-Lewis, Ryan S. Mueller, Brendan Rappazzo, John J. Stachowicz, Fiona Tomas, J. Emmett Duffy
Software: Bo Yang, Tyler Copeland, Luba Reshitnyk
Supervision: Ginny L. Eckert, Carla P. Gomes, C. Drew Harvell, Kevin A. Hovel, Margot Hessing-Lewis, John J. Stachowicz, J. Emmett Duffy
Validation: Bo Yang
Visualization: Bo Yang, Brendan Rappazzo, Luba Reshitnyk
Writing – original draft: Bo Yang
Writing – review & editing: Tyler Copeland, Lia K. Domke, Ginny L. Eckert, Carla P. Gomes, Olivia J. Graham, C. Drew Harvell, Kevin A. Hovel, Margot Hessing-Lewis, Leah Harper, Ryan S. Mueller, Brendan Rappazzo, Luba Reshitnyk, John J. Stachowicz, Fiona Tomas, J. Emmett Duffy

and quantify intensity of disease outbreaks remain major limitations for managing and mitigating the impact of diseases on populations.

Zostera marina, commonly referred to as eelgrass, is a flowering marine plant widespread in coastal areas of the northern hemisphere. Like many other seagrasses, eelgrass lives in intertidal and subtidal inshore waters and forms dense meadows in estuaries and protected coastal seas (Duffy et al., 2013; Moore & Short, 2007). Eelgrass is highly productive and provides habitat for abundant marine invertebrates and fishes (Lefcheck et al., 2019), supports important fisheries (Unsworth et al., 2019), and provides other ecosystem services such as carbon sequestration and water filtration (Costanza et al., 1997). Seagrasses are declining in many regions worldwide due to a variety of stressors, including human impacts and diseases (Dunic et al., 2021; Waycott et al., 2009). Eelgrass is susceptible to eelgrass wasting disease, which is caused by a marine protist, *Labyrinthula zosterae*. The protist invades and kills plant tissue resulting in formation of dark, necrotic lesions (Muehlstein et al., 1991; Ralph & Short, 2002) and has strongly influenced eelgrass dynamics worldwide over the last century (Short et al., 1987; Sullivan et al., 2013). This disease reached epidemic proportions in the 1930s along the North American East Coast and in Europe, killing up to 90% of eelgrass (Addy & Aylward, 1944), and continues to threaten eelgrass recovery worldwide (Short et al., 1987). Rapid loss of eelgrass in New England in the 1980s (Short et al., 1987) and in the northeastern Pacific more recently have also been associated with wasting disease (Groner et al., 2021).

However, eelgrass wasting disease outbreaks are rarely quantified. Common methods of sampling individual eelgrass leaves and scoring the extent of wasting disease lesions are too labor-intensive for widespread assessment of disease outbreaks, especially at the landscape scale (km) and in remote field locations. Furthermore, although the pathogen *L. zosterae* occurs globally (Martin et al., 2016), there is little understanding of regional or geographic patterns in disease dynamics. Efficient assessment of wasting disease is needed to identify baseline infection and outbreak conditions across the geographic range for eelgrass. While molecular approaches such as qPCR assays, culturing, or histology are needed to directly confirm the presence of a pathogen, the expense and infrastructure needed to test a large number of samples may be prohibitively expensive (Burge et al., 2016). Therefore, determining the impact of eelgrass wasting disease at the landscape scale, and predicting future impacts of this disease in association with climate change effects (Aoki et al., 2022), requires multidisciplinary efforts.

With the recent development of microelectronics and image processing algorithms, unoccupied aerial vehicles (UAVs, or drones) are poised to revolutionize regional imaging approaches. Compared to traditional satellite and aerial imaging methods, UAV sensors can achieve high-resolution mapping (<0.05 m) for visible light bands (RGB), which enables unprecedented fine-scale image analysis at the level of individual seagrass leaves over much larger areas than is possible with traditional sampling in situ (Beatty & AokiGrahamYang, 2021). Using programmed autonomous mapping, UAVs can conduct surveys during a short low tide window (about 1 hr) when the upper intertidal area of the bed is exposed (Nahirnick et al., 2019; Yang, Hawthorne, et al., 2019), and with repeatable on-demand imaging capabilities at a lower cost and reduced human effort (Jensen & Mathews, 2016). UAVs can fly stably in windy coastal areas, for example, 25 km/hr (Hardin et al., 2019), and capture imagery during cloudy days, which may impede aerial or satellite remote sensing.

Here, we present a novel interdisciplinary method to greatly expand assessment of the local and regional health of seagrass meadows by integrating on-the-ground ecological approaches with UAV remote sensing and geospatial analysis. We test the ability of UAV low-altitude mapping to reliably detect eelgrass wasting disease across a broad range of sites. UAV fieldwork was conducted simultaneously with in situ sampling for 12 sites in Alaska (AK), British Columbia (BC), and California (CA). Previous studies used remotely sensed leaf index to estimate agriculture production and biomass (Gitelson et al., 2003). We further developed object-oriented image analysis to generate a map of Green Leaf Area Index (G-LAI) over an entire seagrass meadow from high resolution UAV imagery. G-LAI represents the density of the area classified as seagrass that is green in color, indicating healthy tissue. We measured in situ wasting disease severity by collecting and scanning georeferenced plants and using an artificial intelligence program EeLISA (Eelgrass Lesion Image Segmentation Application (Aoki et al., 2022; Rappazzo et al., 2021)) to classify disease severity (percent of individual leaf area i.e., lesioned) for each leaf. We tested the hypothesis that the fine-scale G-LAI from high-resolution imagery would reflect the severity of disease due to an increased fraction of darkened leaf tissue and tested this relationship spanning 18 degrees of latitude along the Pacific coast of North America. Developing leaf index proxies for the physical manifestations of the disease in organisms can be useful, if well-validated, to increase throughput. If proxies can be assessed remotely, then spatial coverage can be greatly increased.

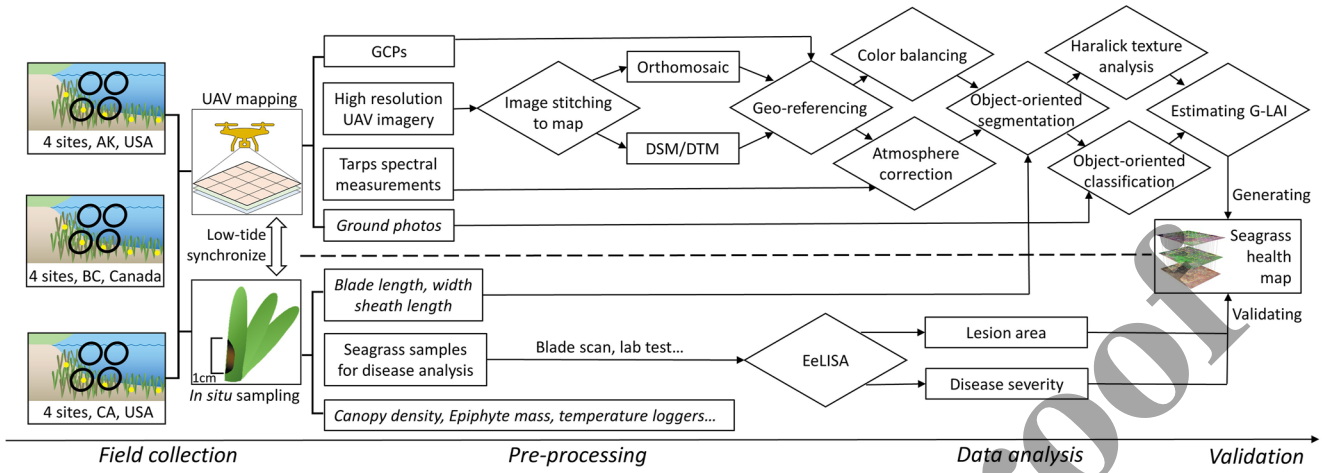

Figure 1. Workflow of the unoccupied aerial vehicle (UAV) and sampling fieldwork, estimating seagrass health map and validation. UAV surveys were conducted at 12 sites in Alaska, British Columbia, and California to derive image-based indices to estimate the spatial extent of eelgrass wasting disease. Images collected from UAV surveys were stitched to create high-resolution orthomosaic images and Digital Surface Model (DSM) using Structure from Motion-Multiview Stereo (SfM-MVS) photogrammetric techniques (Zhang, 2003). Then, mapping products were geo-referenced against GCPs measured from high-performance GNSS system. Meanwhile, the transect tapes (Figure 2) were used to rigorously mark locations on UAV high-resolution imagery. Color balancing was carried out to address the sunlight conditions changing during mapping (Whitehead & Hugenholtz, 2014). The black and white tarps (Figure 2) were used for atmospheric correction through linear transformation (Xu et al.). We used object-oriented image analysis and calculated a Green Leaf Area Index (G-LAI) value that represents the fraction of the total area identified as green seagrass that indicates lack of disease signs.

2. Data and Method

The low-altitude UAV mapping and sampling fieldwork were carried out in 2019 around Prince of Wales Island in Alaska (July 14th to 19th), Central Coast in British Columbia (July 29th to August 3rd), and Bodega and Tomales Bays in California (July 2nd to 6th) following US Federal Aviation Administration (FAA) Part 107 flight guidelines. UAV mapping with temporal flexibility can catch the best low tide to maximize the imaging quality. In this region of the northeast Pacific, coastlines experience mixed semi-diurnal tides; in summer months, lower low water occurs in the morning, exposing the intertidal seagrass beds during spring tides. Data collection targeted spring tides and occurred around 6:30 a.m. (GMT-9) at low tide −32 cm for AK, 7:30 a.m. (GMT-8) at low tide −49 cm for BC, and 7:30 a.m. (GMT-8) at low tide −37.5 cm for CA, with low tide heights relative to mean lower low water. The mapping and image acquisition takes about 1–2 hr. Mapping during the morning with lower sun angles (38°–57° elevation angle) was optimal for minimizing sun glint in UAV imagery (Green et al., 2000) (Figure 1).

The major UAV used is DJI Phantom IV Pro v2 quadcopter equipped with a RGB camera sensor with 12.4 m effective pixels (Stroppiana et al., 2015; Yang, Mansaray, et al., 2019). For each of the eelgrass beds, low-altitude UAV mapping at 60 m/200 ft was conducted under the same fly settings. One challenge for low-altitude marine UAV mapping is that the water surface is often a more homogenous area than land, and the image stitching is challenging or could fail for regions that lack variation (Laliberte & Rango, 2009). To overcome this challenge, we deployed several anchored buoys with taut anchor lines on the near-shore water surface to be used as Ground Control Points (GCPs) during the fieldwork (Figure 2). These contrasting-colored buoys can add matching points to homogeneous water areas to facilitate the image stitching process. Also, a higher overlap ratio, for example, 75% for both front and side overlap ratios, was used in mapping to obtain a larger overlapping area for image stitching and registration. Although the higher overlap ratio leads to a longer mapping time for the same area, we adjusted the mapping route to be parallel with the longer side of the mapping area to minimize the UAV turning points and achieve the best balance between mapping time and coverage. UAV mapping for each eelgrass bed could be completed within 2–3 batteries, with each battery having about 20–25 min of flight time.

In situ eelgrass samples were collected from the third youngest leaf from each plant every four m along a 20 m transect (n = 5 per transect, Figure 2) to measure lesion severity. The sampling locations were marked on the image using six 20 m transect tapes (Figure 2). The eelgrass sampling was part of a long-term study of wasting disease and eelgrass community dynamics, with full details of the sampling methods available elsewhere

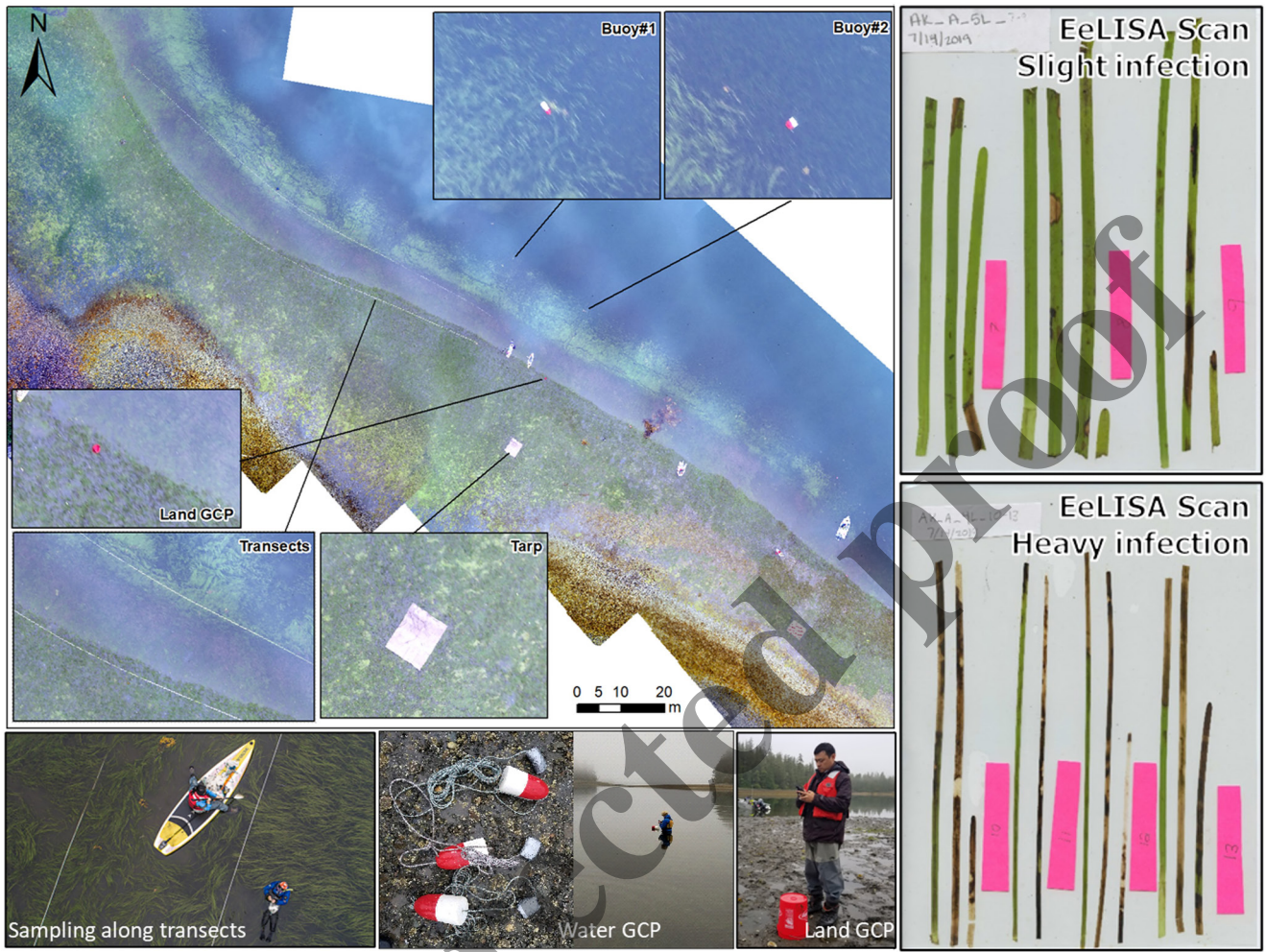

Figure 2. UAV mapping orthomosaic, GCP points on land and water, and tarps for atmosphere correction. Buoys with red/white colors were anchored on the water surface for easier identification on the UAV image. On land, we deployed several orange buckets to be identified as GCPs on the image, and use waterproof Trimble R1 high-performance GNSS to collect coordinates. Two 10 × 8 feet white and black tarps were deployed in all of the UAV mapping sites to be captured by the UAV camera for atmosphere correction. Six 20 m transects at each site, parallel to the shoreline, with three transects at the shoreward edge of the intertidal eelgrass (upper transects) and three transects in the lower portion of the eelgrass bed, closer to the ocean (lower transects). Upper and lower transects were set to be parallel and 5–10 m apart from each other. This sampling design ensured an even spatial distribution of the in situ sampling points. The eelgrass samples were scanned in lab and measure lesion area using EeLISA.

(Aoki et al., 2022). As wasting disease infection progresses, the eelgrass leaves further lose the green leaf area by turning from green to black and brown color (Figure 2) (Duffy et al., 2018). To precisely measure wasting disease severity for different sites among the different seagrass conditions, we used the Eelgrass Lesion Image Segmentation Application (EeLISA), an artificial intelligence program developed by Cornell University (Rappazzo et al., 2021). For each scanned leaf image, EeLISA measured the total lesion area and the total leaf area (including healthy and diseased tissue). The lesion area was divided by the total leaf area to calculate disease severity of each sampling point.

Image analysis includes object-oriented image segmentation, classification for eelgrass patches, and G-LAI estimation. Low altitude UAV mapping provides a high-resolution orthomosaic image and Digital Surface Model (DSM) at 1.5 cm spatial resolution, which enables the object-oriented image analysis at an unprecedented fine scale. For the image segmentation, we considered spectral bands of visible light and used the leaf length to calibrate the scale parameter (object size). The maximum likelihood fitting method was used to determine the object scale against in situ sampling data of leaf length (Yang, Mansaray, et al., 2019). The object scale parameter was iterated from 10 to 180 and compared the object size to the longest leaf length from sampling (Yang, Mansaray,

et al., 2019). The method calculated mean scale parameter 95 for AK, 85 for BC, and 65 for CA. The shape and compactness were fit to 0.5 and 0.2 using same maximum likelihood approach. The scale parameter is weighted with shape parameters (with separation of shape and compactness parameters) to minimize the fractal borders of the objects. In the results, each segmented object is treated as one plant, or a cluster of plants of eelgrass with similar characteristics.

After segmentation, the supervised classification was performed on the segmentation results to extract the eelgrass objects from unvegetated objects within each scene. Based on fieldwork photos and in situ sampling locations, a set of objects that have been ground-truthed as eelgrass were selected as training data, and all eelgrass belonging to this class was extracted. Other classes were also selected on the image based on the fieldwork records, including water area, sand/bare soil, shore, and other non-seagrass features. Haralick texture analysis tool was used to distinguish the seagrass meadows from sand and algae due to the different textures (Laliberte & Rango, 2009).

The G-LAI was calculated based on the object-oriented segmentation and classification results, defined as the green leaf area per object total area classified as seagrass (Watson, 1947). Roth et al. (2018) proposed a method to estimate LAI based on RGB images and viewing geometry from high-resolution UAV mapping, and their validation results suggest this method achieved strong results ($R^2 > 0.9$) compared with in situ ground truth measurements (Roth et al., 2018). We follow the methods for the segmentation of green vegetation like seagrass, including Normalized Green Red Difference Index (NGRDI) (Bassine et al., 2019), Excess Green (ExG) (Meyer & Neto, 2008), and Green Leaf Index (GLI) (Louhaichi et al., 2001). As wasting disease infection leads to the loss of greenness, GLI was used to extract the green seagrass portion and calculate G-LAI (Liu & Wang, 2018).

The G-LAI method aims to estimate a whole canopy rather than the leaf area of a single leaf. The image shows a canopy from a specific viewpoint and area; therefore, it is related to a certain viewing geometry based on zenith and azimuth angle. In our case study, UAV mapping was controlled by an autonomous mapping application with recorded in nadir view pixels. The small scale variation of zenith angle can be calculated by the DSM from UAV mapping products. The fraction of eelgrass pixels in each object was calculated as the ratio between the extracted seagrass green leaf area and total number of pixels. Figure 3 shows the UAV mapping orthomosaic for 12 eelgrass beds and one example (Nossuk) of object-oriented image processing. We utilized Esri Drone2Map for image pre-processing and stitching, Esri ArcGIS and Trimble eCognition for image processing, and R Studio for statistical analysis.

3. Results

Three statistical models were adapted to test the regional and global relationship between G-LAI and wasting disease severity. For the per site linear regression model, UAV-derived G-LAI was strongly predicted by eelgrass disease severity (Table 1, Figure 4) for all 12 sites in AK, BC, and CA, demonstrating a negative relationship between G-LAI and in situ wasting disease severity. The G-LAI estimated from the object-oriented analysis explains 47%–58% of the total variation in wasting disease for Alaska, and about 30% for British Columbia and California (Table 1).

Two global models (all sites from three regions) were conducted to predict severity and presence of disease signs using G-LAI (Table 1). The first is a logistic regression model that test disease presence (yes/no) with G-LAI values, we found that this model is also statistically significant, with coefficient -4.07 ± 0.61; $Z = -6.648$, $p < 0.001$ (Table 1). Based on the model we calculate threshold value of G-LAI is 0.6144 for 50% disease prevalence, hence such areas with a G-LAI below this threshold can be rapidly detected more likely than not to have disease present.

Also, a global linear model was constructed to predict disease severity from G-LAI (Table 1). The model achieved statistical significance, but the overall R^2 decreased to 0.231, considerably lower than the site by site models, suggesting differences among regions in the severity—G-LAI relationship. Indeed, when we added region as a fixed effect (Allison, 2002), explanatory power improved somewhat to R^2 of 0.289 (Table 1). Bodega Bay and Tomales Bay were modeled separately because they have different topography and environmental conditions (DuBois et al., 2022) (see locations in Figure 4).

Visually, orthomosaic imagery of the eelgrass beds generally showed reduced G-LAI around in situ sampling sites where disease was detected (Figure 5). In Nossuk (Figure 5c) the lower transect (close to the water) displays

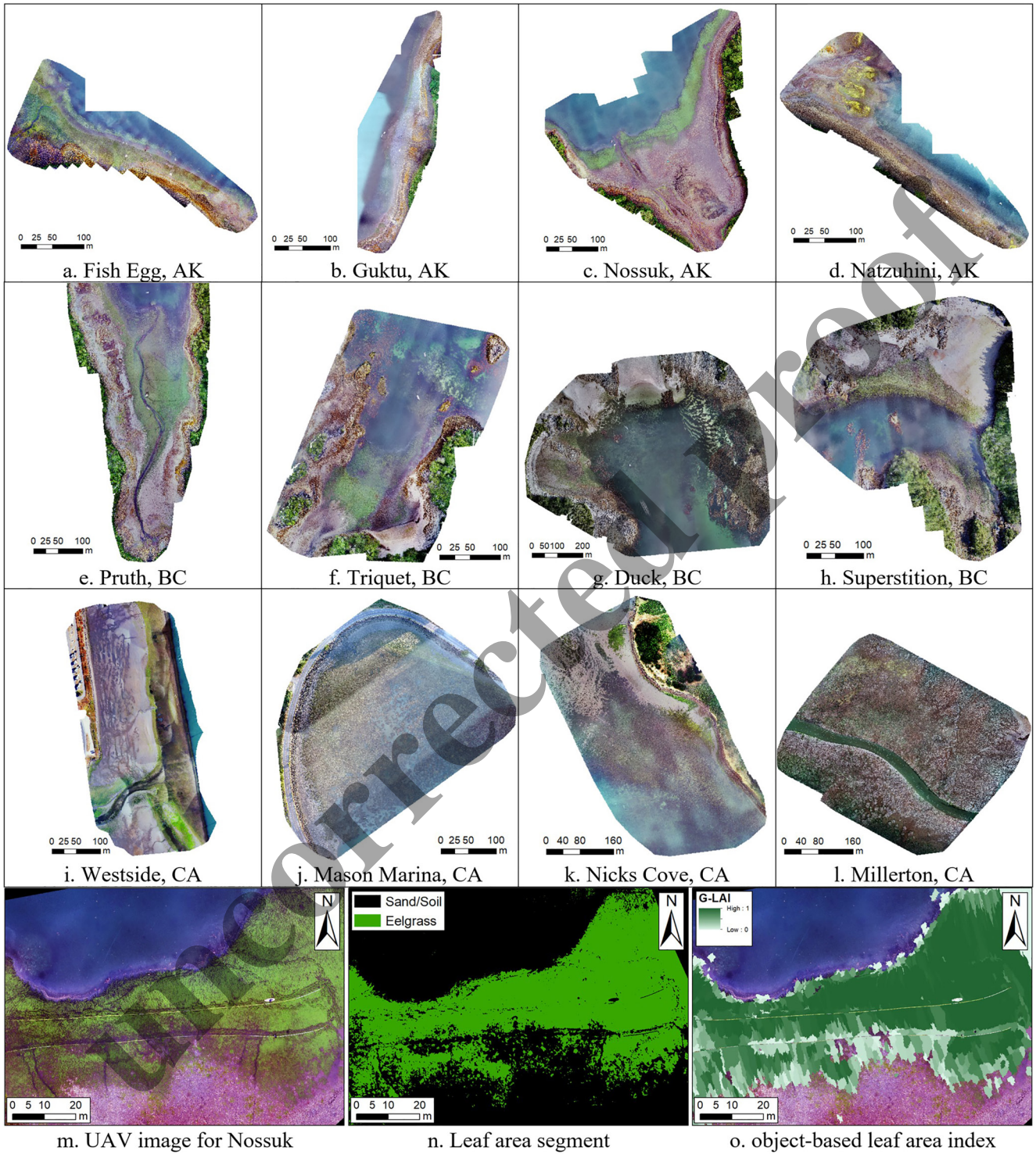

Figure 3. UAV mapping processing products for Alaska: (a) Fish Egg on July 14th; (b) Guktu on July 15th; (c) Nossuk on July 16th; (d) Natzuhini on July 17th; British Columbia: (e) Pruth on July 29th; (f) Triquet on August 1st; (g) Goose on August 2nd; (h) Superstition on August 3rd; and California: (i) Westside on July 2nd; (j) Mason Marina on July 3rd; (k) Nicks Cove on July 5th; (l) Millerton on July 4th. (m–o),Processing example for Nossuk (m), original UAV orthomosaic imagery, (n), extracted green leaf area, o), choropleth map showing G-LAI calculated for each object; higher G-LAI areas are shown in dark green color while lower G-LAI areas in light green color.

Table 1
Statistical Models Between UAV Mapping G-LAI and in Situ Sampling Disease Severity

Per site regression		Lat(°)	Long(°)	R	R^2	Coefficient	SE	p-value
AK	Fish Egg	55.496	−133.168	0.691	0.478	−1.05	0.207	0.0001
	Guktu	55.739	−133.312	0.758	0.575	−7.00	1.137	0.0001
	Nossuk	55.707	−133.343	0.722	0.521	−3.44	0.623	0.0001
	Natzuhini	55.249	−132.881	0.708	0.501	−3.30	0.623	0.0001
BC	Duck	51.924	−128.470	0.562	0.316	−2.70	0.752	0.0012
	Superstition	51.894	−128.23 5	0.582	0.339	−1.50	0.395	0.0007
	Triquet	51.808	−128.237	0.609	0.371	−0.69	0.169	0.0003
	Pruth Bay	51.645	−128.119	0.401	0.161	−0.31	0.134	0.0282
CA	Nicks Cove	38.205	−122.927	0.587	0.345	−1.85	0.483	0.0006
	Millerton	38.105	−122.846	0.589	0.347	−2.29	0.596	0.0006
	Mason Marina	38.333	−123.059	0.560	0.314	−1.13	0.317	0.0013
	Westside	38.319	−123.054	0.596	0.356	−1.30	0.33	0.0005

Global regression	R	R^2	Coefficient	SE	p-value
G-LAI without fixed effect	0.481	0.231	−0.209	0.02	<0.000
G-LAI with fixed effect			−0.258	0.02	<0.000
Dummy BC (fixed effect)	0.537	0.289	0.0545	0.01	<0.000
Dummy Bodega (fixed effect)			0.0350	0.01	0.011
Dummy Tomales (fixed effect)			−0.0084	0.01	0.533

Logistic regression	z value	Coefficient	SE	p-value
G-LAI	−6.648	−4.0708	0.6123	<0.000
Intercept	5.968	3.0011	0.5028	<0.000

a better leaf condition, visible in the image as greener color, than the upper transect. Note in the middle part of the upper transect (close to the land) in Nossuk (Figure 5c), there is a large increase in disease severity detected in the in situ samples as indicated by the largest circles in the middle part. Meanwhile, the UAV image shows the same large loss of the green leaf area at the same area. This leaf area pattern reflected in the UAV imagery has a close correlation with the in situ sampling results. In the maps of Fish Egg (Figure 5a) and Guktu (Figure 5b) similar patterns are observed. Sampling points with higher disease severity correspond to non-green sections of the image, explaining the negative relationship of severity to the green leaf area.

4. Conclusions and Discussion

We highlight a novel low-altitude UAV mapping and image analysis method that can detect variation in eelgrass wasting disease severity and presence, validated by in situ sampling, over 12 sites spanning much of the North American west coast across 18 degrees of latitude. The ability of UAV mapping to predict eelgrass disease severity was statistically significant for 12 sites, and explained an average 38.5% of variation in disease severity. This suggests that it is feasible to use UAV high-resolution images and geospatial image analysis to extend the spatial scale of mapping eelgrass wasting disease. The performance of G-LAI as an indicator for the presence and severity of wasting disease was robust across a wide range of eelgrass and disease conditions, including differences in plant morphology and epiphyte load, which have been associated with wasting disease severity in prior studies (Groner et al., 2016). The in situ sampling indicates lower epiphyte/fouling loads and higher water clarity in Alaska sites, which might be one explanation for the variation in predictive ability across those sites. The method is especially applicable for areas with higher infection by disease and lower epiphyte cover, such as AK sites, since both disease and epiphyte load reduce G-LAI. Our findings suggest that drone mapping of coastal plants could facilitate the feasibility of large-scale spatially-explicit disease risk assessments in nearshore habitats and further our understanding of seagrass meadow spatial-temporal dynamics.

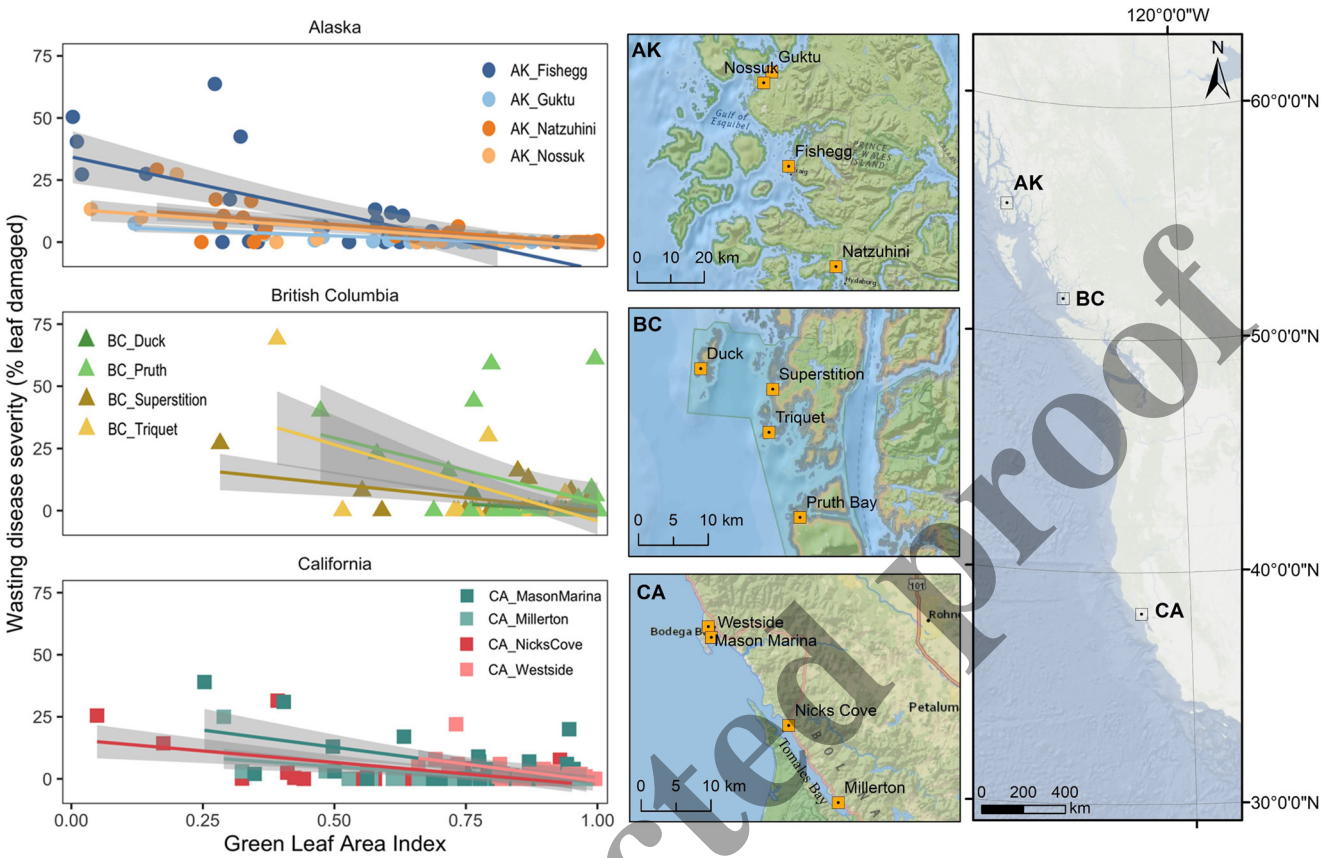

Figure 4. Regression results and scatter plot between UAV eelgrass G-LAI and in situ disease severity for 12 sites spanning 18 degrees of latitude. Sampling eelgrass beds including 4 sites in Prince of Wales Island in Alaska (USA), 4 sites in Central Coast in British Columbia (Canada), and 4 sites in Bodega and Tomales Bays in California (USA).

Diseases of marine organisms are increasing in many regions worldwide, with important consequences for ecosystems and humanity (Burge et al., 2014; Harvell et al., 2002). Despite increasing interest in seagrass meadow conservation, only one-tenth of the estimated global extent of seagrass meadows has been fully mapped (Dunic et al., 2021; McKenzie et al., 2020) and the influence of wasting disease on contemporary regional and global seagrass declines is not well understood. Recent evidence further suggests that wasting disease outbreaks are likely to increase with warming temperatures from climate change (Aoki et al., 2022; Bull et al., 2012; Groner et al., 2021), magnifying the need for rapid disease assessment at the landscape scale. Our method provides new opportunities to investigate environmental drivers and ecological impacts of eelgrass wasting disease at the landscape scale and across the geographic range of eelgrass. By implementing UAV mapping, scientists and managers may be able to identify wasting disease outbreaks and target limited monitoring resources. Although interventions to treat seagrass wasting disease are in their infancy, worsening disease outbreaks may indicate impending eelgrass decline (Aoki et al., 2022; Groner et al., 2021). Rapid and large-scale assessment of seagrass health by UAVs can enable managers to include disease as a key factor driving seagrass dynamics and aid in pinpointing resilient, healthy meadows to conserve. As climate change accelerates, potentially increasing the frequency and severity of disease outbreaks (Aoki et al., 2022; Burge et al., 2014), new approaches such as those tested here will improve our ability to understand, forecast and manage ecological change.

Most of our sites were mapped simultaneously with in situ fieldwork, and this manifested the spatial correlation between in situ and UAV estimates. Meanwhile, we found temporal correlations when G-LAI and in situ sampling measurements were separated by some time, given the orientation of seagrass leaves may change with currents, tides, and water depth, the canopy location remains stable. For example, one California site (Millerton Point) was mapped by UAV on July 4, while the in situ samplings were performed on July 31, and the correlation between G-LAI and disease severity was as strong as at other sites. Asynchronous mapping would allow for

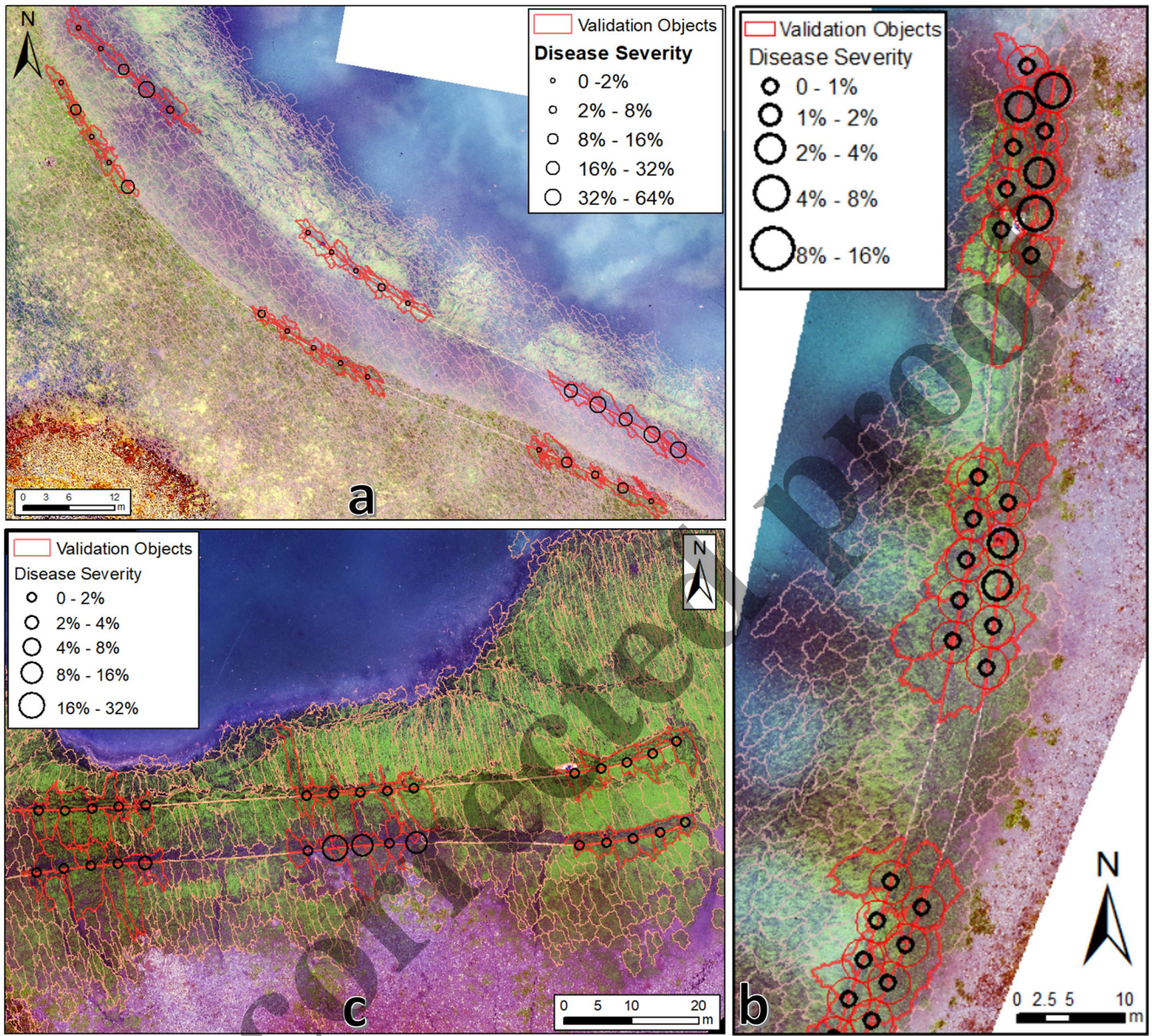

Figure 5. The sampling disease severity overlay with eelgrass objects (in red) for Alaska sites: (a) Fish Egg; (b) Guktu; (c) Nossuk. The sampling disease severity values are coded in different-sized symbols (in black) with larger circles corresponding to more severe lesions along both upper and lower transects. Lesion severity is calculated as the leaf area covered by lesion divided by total leaf area.

even greater flexibility in implementing UAV methods to monitor disease, since poor flying conditions would not constrain sampling dates. The success of this method demonstrates how UAV mapping can upscale disease surveillance efforts by augmenting conventional fieldwork and providing predictions at spatial and temporal scales that previously were not achievable due to limitations of conventional satellite imagery methods (Yang, Hawthorne, et al., 2019).

The primary drone used in this study is DJI Phantom IV Pro, which is a reliable and cost-effective solution for coastal mapping (Beatty & AokiGrahamYang, 2021; Duffy et al., 2018). Its main advantage is the visible light bands with high resolution and water penetration ability for intertidal mapping (Lee et al., 2013). We also used a Parrot Bluegrass UAV with Sequoia multi-spectral sensor (Yang, Hawthorne, et al., 2019). Its near-infrared (NIR) band can detect biomass but with coarser resolution and weaker water penetration ability. Moreover, we note that although the direction and fit of the association is consistent across regions, the slope of the relationship varies somewhat both among and within regions (Figure 2). Currently, this limits the precise application of the G-LAI

as a general indicator of disease severity across sites. However, future studies could assess correlates of this variation in slope such as epiphyte load, water clarity, length of plants. Number of leaves per shoot, and temperature to develop a relationship that could predict disease severity from remotely sensed data alone. Moreover, our G-LAI metric may be a better estimate of meadow condition than in situ sampling of individual blades because it accounts for green leaf area across the entire surveyed area, while sampled in situ lesion severity occurred only on the third youngest leaf of each plant and sampled a much smaller number of plants. Regardless, we note that the combination of in situ leaf measurements and UAV sampling allows expanding the spatial scope of sampling to broader areas within a site, extending our understanding of disease patterns far beyond that obtainable with leaf sampling alone. This application could easily be extended to monitoring other plant diseases that noticeably discolor leaf surfaces (Gitelson et al., 2003).

Conflict of Interest

The authors declare no conflicts of interest relevant to this study.

Data Availability Statement

All data used to produce this paper are available at Mendeley Data "UAV imaging for quantifying eelgrass wasting disease for AK, BC, and CA", Mendeley Data, V1, https://doi.org/10.17632/chbptxsjm6.1.

Acknowledgments
This material is based upon work supported by the U.S. National Science Foundation (Awards OCE-1829890, OCE-1829922, OCE-1829921, OCE-1829992, OCE-1600230, OCE-1635716). This is contribution 123 from the Smithsonian's MarineGEO and Tennenbaum Marine Observatories Network. Funding for MHL and LR from the Hakai Institute and Tula Foundation.

References

Addy, C. E., & Aylward, D. A. (1944). Status of eelgrass in Massachusetts during 1943. *Journal of Wildlife Management*, *8*(4), 269–275. https://doi.org/10.2307/3796019

Allison, D. (2002). *Bias in fixed-effects Cox regression with dummy variables. Manuscript*. Department of Sociology, University.

Aoki, L. R., Rappazzo, B., Beatty, D. S., Domke, L. K., Eckert, G. L., Eisenlord, M. E., et al. (2022). Disease surveillance by artificial intelligence links eelgrass wasting disease to ocean warming across latitudes. *Limnology & Oceanography*, *67*(7), 1577–1589. https://doi.org/10.1002/lno.12152

Bassine, F. Z., Errami, A., & Khaldoun, M. (2019). Vegetation recognition based on UAV image color index. In *2019 IEEE international conference on environment and electrical engineering and 2019 IEEE industrial and commercial power systems Europe (EEEIC/I&CPS Europe)* (pp. 1–4).

Beatty, D. S., & AokiGrahamYang, L. R. O. J. B. (2021). The future is big—And small: Remote sensing enables cross-scale comparisons of microbiome dynamics and ecological consequences. *mSystems*, *6*(6). https://doi.org/10.1128/MSYSTEMS.01106-21

Bull, J. C., Kenyon, E. J., & Cook, K. J. (2012). Wasting disease regulates long-term population dynamics in a threatened seagrass. *Oecologia*, *169*(1), 135–142. https://doi.org/10.1007/s00442-011-2187-6

Burge, C. A., Friedman, C. S., Getchell, R., House, M., Lafferty, K. D., Mydlarz, L. D., et al. (2016). Complementary approaches to diagnosing marine diseases: A union of the modern and the classic. *Philosophical Transactions of the Royal Society of London B Biological Sciences*, *371*(1689), 20150207. https://doi.org/10.1098/rstb.2015.0207

Burge, C. A., Mark Eakin, C., Friedman, C. S., Froelich, B., Hershberger, P. K., Hofmann, E. E., et al. (2014). Climate change influences on marine infectious diseases: Implications for management and society. *Annual Review of Marine Science*, *6*(1), 249–277. https://doi.org/10.1146/annurev-marine-010213-135029

Costanza, R., D'Arge, R., de Groot, R., Farber, S., Grasso, M., Hannon, B., et al. (1997). The value of the world's ecosystem services and natural capital. *Nature*, *387*(6630), 253–260. https://doi.org/10.1038/387253a0

DuBois, K., Pollard, K. N., Kauffman, B. J., Williams, S. L., & Stachowicz, J. J. (2022). Local adaptation in a marine foundation species: Implications for resilience to future global change. *Global Change Biology*, *28*(8), 2596–2610. https://doi.org/10.1111/gcb.16080

Duffy, J. E., Hughes, A. R., & Moksnes, P. O. (2013). Ecology of seagrass communities. In M. D. Bertness, J. F. Bruno, B. R. Silliman, & J. J. Stachowicz (Eds.), *Marine community ecology and conservation* (pp. 271–297).

Duffy, J. P., Pratt, L., Anderson, K., Land, P. E., & Shutler, J. D. (2018). Spatial assessment of intertidal seagrass meadows using optical imaging systems and a lightweight drone. *Estuarine, Coastal and Shelf Science*, *200*, 169–180. https://doi.org/10.1016/j.ecss.2017.11.001

Dunic, J. C., Brown, C. J., Connolly, R. M., Turschwell, M. P., & Côté, I. M. (2021). Long-term declines and recovery of meadow area across the world's seagrass bioregions. *Global Change Biology*.

Gitelson, A. A., Vina, A., Arkebauer, T. J., Rundquist, D. C., Keydan, G., & Leavitt, B. (2003). Remote estimation of leaf area index and green leaf biomass in maize canopies. *Geophysical Research Letters*, *30*(5). https://doi.org/10.1029/2002gl016450

Glidden, C. K., Field, L. C., Bachhuber, S., Hennessey, S. M., Cates, R., Cohen, L., et al. (2022). Strategies for managing marine disease. *Ecological Applications*, *32*(7), e2643.

Green, E., Mumby, P., Edwards, A., & Clark, C. (2000). *Remote sensing: Handbook for tropical coastal management*. United Nations Educational, Scientific and Cultural Organization (UNESCO).

Groner, M. L., Burge, C., Kim, C., Rees, E., Van Alstyne, K., Yang, S., et al. (2016). Plant characteristics associated with widespread variation in eelgrass wasting disease. *Diseases of Aquatic Organisms*, *118*(2), 159–168. https://doi.org/10.3354/dao02962

Groner, M. L., Eisenlord, M., Yoshioka, R., Fiorenza, E., Dawkins, P., Graham, O., et al. (2021). Warming sea surface temperatures fuel summer epidemics of eelgrass wasting disease. *Marine Ecology Progress Series*, *679*, 47–58. https://doi.org/10.3354/meps13902

Hardin, P. J., Lulla, V., Jensen, R. R., & Jensen, J. R. (2019). Small Unmanned Aerial Systems (sUAS) for environmental remote sensing: Challenges and opportunities revisited. *GIScience and Remote Sensing*, *56*(2), 309–322. https://doi.org/10.1080/15481603.2018.1510088

Harvell, C. D., Mitchell, C. E., Ward, J. R., Altizer, S., Dobson, A. P., Ostfeld, R. S., & Samuel, M. D. (2002). Climate warming and disease risks for terrestrial and marine biota. *Science*, *296*(5576), 2158–2162. https://doi.org/10.1126/science.1063699

Jensen, J. L. R., & Mathews, A. J. (2016). Assessment of image-based point cloud products to generate a bare Earth surface and estimate canopy heights in a woodland ecosystem. *Remote Sensing*, *8*(1), 50. https://doi.org/10.3390/rs8010050

Laliberte, A. S., & Rango, A. (2009). Texture and scale in object-based analysis of subdecimeter resolution unmanned aerial vehicle (UAV) imagery. *IEEE Transactions on Geoscience and Remote Sensing*, *47*(3), 1–10. https://doi.org/10.1109/tgrs.2008.2009355

Lee, Z., Hu, C., Shang, S., Du, K., Lewis, M., Arnone, R., & Brewin, R. (2013). Penetration of UV-visible solar radiation in the global oceans: Insights from ocean color remote sensing. *Journal of Geophysical Research: Oceans*, *118*(9), 4241–4255. https://doi.org/10.1002/jgrc.20308

Lefcheck, J. S., Hughes, B. B., Johnson, A. J., Pfirrmann, B. W., Rasher, D. B., Smyth, A. R., et al. (2019). Are coastal habitats important nurseries? A meta-analysis. *Conservation Letters*, *12*(4), e12645. https://doi.org/10.1111/conl.12645

Liu, X., & Wang, L. (2018). Feasibility of using consumer-grade unmanned aerial vehicles to estimate leaf area index in mangrove forest. *Remote Sensing Letters*, *9*(11), 1040–1049. https://doi.org/10.1080/2150704x.2018.1504339

Lopez-Calderon, J. M., Riosmena-Rodríguez, R., Torre, J., Meling, A., & Basurto, X. (2016). Zostera marina meadows from the gulf of California: Conservation status. *Biodiversity & Conservation*, *25*(2), 261–273. https://doi.org/10.1007/s10531-016-1045-6

Louhaichi, M., Borman, M. M., & Johnson, D. E. (2001). Spatially located platform and aerial photography for documentation of grazing impacts on wheat. *Geocarto International*, *16*(1), 65–70. https://doi.org/10.1080/10106040108542184

Martin, D. L., Chiari, Y., Boone, E., Sherman, T. D., Ross, C., Wyllie-Echeverria, S., et al. (2016). Functional, phylogenetic and host-geographic signatures of Labyrinthula spp. provide for putative species delimitation and a global-scale view of seagrass wasting disease. *Estuaries and Coasts*, *39*(5), 1403–1421. https://doi.org/10.1007/s12237-016-0087-z

McKenzie, L. J., Nordlund, L. M., Jones, B. L., Cullen-Unsworth, L. C., Roelfsema, C., & Unsworth, R. K. F. (2020). The global distribution of seagrass meadows. *Environmental Research Letters*, *15*(7), 74041. https://doi.org/10.1088/1748-9326/ab7d06

Meyer, G. E., & Neto, J. C. (2008). Verification of color vegetation indices for automated crop imaging applications. *Computers and Electronics in Agriculture*, *63*(2), 282–293. https://doi.org/10.1016/j.compag.2008.03.009

Moore, K. A., & Short, F. T. (2007). Zostera: Biology, ecology, and management. In *Seagrasses: Biology, ecology and conservation* (pp. 361–386). Springer.

Muehlstein, L. K., Porter, D., & Short, F. T. (1991). Labyrinthula zosterae sp. nov., the causative agent of wasting disease of eelgrass, Zostera marina. *Mycologia*, *83*(2), 180–191. https://doi.org/10.2307/3759933

Nahirnick, N. K., Reshitnyk, L., Campbell, M., Hessing-Lewis, M., Costa, M., Yakimishyn, J., & Lee, L. (2019). Mapping with confidence; delineating seagrass habitats using Unoccupied Aerial Systems (UAS). *Remote Sensing in Ecology and Conservation*, *5*(2), 121–135. https://doi.org/10.1002/rse2.98

Ralph, P. J., & Short, F. T. (2002). Impact of the wasting disease pathogen, Labyrinthula zosterae, on the photobiology of eelgrass Zostera marina. *Marine Ecology Progress Series*, *226*, 265–271. https://doi.org/10.3354/meps226265

Rappazzo, B. H., Eisenlord, M. E., Graham, O. J., Aoki, L. R., Dawkins, P. D., Harvell, D., & Gomes, C. (2021). EeLISA: Combating global warming through the rapid analysis of eelgrass wasting disease. In *Proceedings of the AAAI conference on artificial intelligence* (Vol. 35, pp. 15156–15165).

Roth, L., Aasen, H., Walter, A., & Liebisch, F. (2018). ISPRS journal of photogrammetry and remote sensing extracting leaf area index using viewing geometry effects — A new perspective on high-resolution unmanned aerial system photography. *ISPRS Journal of Photogrammetry and Remote Sensing*, *141*, 161–175. https://doi.org/10.1016/j.isprsjprs.2018.04.012

Short, F. T., Muehlstein, L. K., & Porter, D. (1987). Eelgrass wasting disease: Cause and recurrence of a marine epidemic. *Biology Bulletin*, *173*(3), 557–562. https://doi.org/10.2307/1541701

Stroppiana, D., Migliazzi, M., Chiarabini, V., Crema, A., Musanti, M., Franchino, C., & Villa, P. (2015). Rice yield estimation using multispectral data from UAV: A preliminary experiment in northern Italy. In *2015 IEEE international geoscience and remote sensing symposium (IGARSS)* (pp. 4664–4667). IEEE.

Sullivan, B. K., Sherman, T. D., Damare, V. S., Lilje, O., & Gleason, F. H. (2013). Potential roles of Labyrinthula spp. in global seagrass population declines. *Fungal Ecology*, *6*(5), 328–338. https://doi.org/10.1016/j.funeco.2013.06.004

Unsworth, R. K. F., Nordlund, L. M., & Cullen-Unsworth, L. C. (2019). Seagrass meadows support global fisheries production. *Conservation Letters*, *12*(1), e12566. https://doi.org/10.1111/conl.12566

Watson, D. J. (1947). Comparative physiological studies on the growth of field crops: I. Variation in net assimilation rate and leaf area between species and varieties, and within and between years. *Annals of Botany*, *11*(1), 41–76. https://doi.org/10.1093/oxfordjournals.aob.a083148

Waycott, M., Duarte, C. M., Carruthers, T. J. B., Orth, R. J., Dennison, W. C., Olyarnik, S., et al. (2009). Accelerating loss of seagrasses across the globe threatens coastal ecosystems. *Proceedings of the National Academy of Sciences*, *106*(30), 12377–12381. https://doi.org/10.1073/pnas.0905620106

Whitehead, K., & Hugenholtz, C. H. (2014). Remote sensing of the environment with small unmanned aircraft systems (UASs), Part 1: A review of progress and challenges. *Journal of Unmanned Vehicle Systems*, *2*(03), 69–85. https://doi.org/10.1139/juvs-2014-0006

Xu, M., Liu, H., Beck, R., Lekki, J., Yang, B., Shu, S., et al. (2019). Regionally and locally adaptive models for retrieving Chlorophyll-a concentration in inland waters from remotely Sensed multispectral and hyperspectral imagery. Retrieved from ieeexplore.ieee.org

Yang, B., Hawthorne, T. L., Torres, H., & Feinman, M. (2019). Using object-oriented classification for coastal management in the East central coast of Florida: A quantitative comparison between UAV, satellite, and aerial data. *Drones*, *3*, 60. https://doi.org/10.3390/drones3030060

Yang, L., Mansaray, L. R., Huang, J., & Wang, L. (2019). Optimal segmentation scale parameter, feature subset and classification algorithm for geographic object-based crop recognition using multisource satellite imagery. *Remote Sensing*, *11*(5), 514. https://doi.org/10.3390/rs11050514

Zhang, L. (2003). Shape and motion under varying illumination: Unifying structure from motion, photometric stereo, and multiview stereo. In *Proceedings ninth IEEE international conference on computer vision* (pp. 618–625).